Lithuanian Journal of Physics, Vol. **57**, No. 3, pp. 183–193 (2017)

PREPARATION, STRUCTURE, SURFACE AND IMPEDANCE ANALYSIS OF $Na_2Zn_{0.5}Mn_{0.5}P_2O_7$ CERAMICS

V. Venckutė [a], A. Dindune [b], D. Valdniece [b], A. Krumina [b], M. Lelis [c], V. Jasulaitienė [d], A. Maneikis [d], S. Daugėla [a], T. Šalkus [a], A. Kežionis [a], and A.F. Orliukas [a]

[a] *Faculty of Physics, Vilnius University, Saulėtekio 9/3, LT-10222 Vilnius, Lithuania*
[b] *Institute of Inorganic Chemistry, Riga Technical University, Paula Valdena 3/7, LV-1048 Riga, Latvia*
[c] *Center for Hydrogen Energy Technologies, Lithuanian Energy Institute, Breslaujos 3, LT-44403 Kaunas, Lithuania*
[d] *National Center for Physical Sciences and Technology, Saulėtekio 3, LT-10222 Vilnius, Lithuania*
E-mail: saulius.daugela@ff.vu.lt

Received 16 March 2017; revised 15 May 2017; accepted 15 June 2017

The $Na_2Zn_{0.5}Mn_{0.5}P_2O_7$ powder was prepared by the solid state reaction method. The powder structure was studied by X-ray diffraction (XRD) in the temperature range from room temperature (RT) to 520 K. The results of XRD measurements show that the obtained $Na_2Zn_{0.5}Mn_{0.5}P_2O_7$ is a mixture of two phases: $Na_2MnP_2O_7$, which crystallizes in the triclinic space group $P\bar{1}$, and $Na_2ZnP_2O_7$, which crystallizes in the tetragonal space group $P4_2/mmm$. The chemical compositions of the powder and ceramic samples were investigated by an energy dispersive X-ray spectrometer (EDX) and X-ray fluorescence spectroscopy (XFS). The surface of ceramics was examined by X-ray photoelectron spectroscopy (XPS). The electrical conductivity and dielectric permittivity of the ceramics were investigated from RT to 700 K in the frequency range 10–10^9 Hz. The relaxational dispersion of electrical conductivity in the investigated frequency and temperature range was found.

Keywords: sodium, pyrophosphate, crystal structure, conductivity, dielectric permittivity

PACS: 82.45.Xy, 84.37.+q, 79.60.-i

1. Introduction

Further progress in the development of secondary batteries for electrochemical energy storage requires the development of new ion-conducting materials. Li-ion batteries have dominated during the last decades due to their high power and energy density [1–3]. However, the high cost and scarcity of lithium reserves have resulted in the pursuit of alternative energy storage materials [1]. Among various alternatives to the Li-ion batteries, the sodium-ion batteries are promising due to the abundant resources and low cost of sodium [4]. Some Na^+-conducting compounds of the pyrophosphate family are attractive cathode materials for sodium ion batteries [4–14]. Sodium-based pyrophosphate compounds such as $Na_2MP_2O_7$ (M = Mn, Fe, Co, Zn) are presently under intensive investigation. The β-$Na_2MnP_2O_7$ polymorph [5, 6] and $NaFeP_2O_7$ [7–10] crystallize in the triclinic structure (space group $P\bar{1}$), $Na_2CoP_2O_7$ crystallizes in the orthorhombic space group $Pna2_1$ [11], and $Na_2ZnP_2O_7$ crystallizes in the tetragonal space group $P4_2/mmm$ [12]. Charge/discharge capacity and redox potential measurements of these compounds were performed [6, 8, 13, 14]. The galvanostatic cycling of β-$Na_2MnP_2O_7$ at the rate C/20 showed its

discharge capacity approaching 80 mAh/g along with the highest ever Mn^{3+}/Mn^{2+} redox potential of 3.6 V [6]. The $Na_2CoP_2O_7$ delivers a reversible capacity close to 80 mAh/g involving the Co^{3+}/Co^{2+} redox activity with an average potential of 3 V [13]. The $Na_2FeP_2O_7$ cathode was found to be electrochemically active, delivering a reversible capacity of 82 mAh/g with the Fe^{3+}/Fe^{2+} redox potential around 3 V (vs Na/Na^+) [8]. Attempts to improve the electrochemical properties of materials involved various cationic substitutions in the pyrophosphates by synthesizing new compounds, namely $Na_2Fe_{0.5}Mn_{0.5}P_2O_7$ [4], $Na_{2-x}(Fe_{1-y}Mn_y)P_2O_7$ ($0 \le y \le 1$) [7], $NaCsMnP_2O_7$ and $NaCsMn_{0.35}Cu_{0.65}P_2O_7$ [5]. The charge/discharge measurements indicate that the substituted $Na_2Fe_{0.5}Mn_{0.5}P_2O_7$ is chemically active with a reversible capacity of ~80 mAh/g at the C/20 rate with an average redox potential of 3.2 V (vs Na/Na^+) [14]. The measurements of structure and electrochemical properties of the abovementioned pyrophosphates were performed at room temperature (RT). The investigation of the crystal structure and electrical properties, and the differential thermal analysis of $Na_2MnP_2O_7$ [15] and $NaCsZn_{0.5}Mn_{0.5}P_2O_7$ [16] ceramics showed structural phase transitions taking place at elevated temperature. At 660 K the phase transition in the $Na_2MnP_2O_7$ compound leads to the anomalies of dielectric permittivity, electric conductivity and the change of activation energy from 0.78 eV at $T \le 660$ K to 0.68 eV at $T \ge 660$ K. The authors of Ref. [17] show that relaxation processes in the polycrystalline $Na_2ZnP_2O_7$ are caused by the Na^+-ion motion and their activation energy of 0.94 eV is almost the same as the activation energy for the conductivity. At 600 K the values of the conductivity were $3.7 \cdot 10^{-3}$ S/m and $4.98 \cdot 10^{-6}$ S/m for $Na_2MnP_2O_7$ [15] and $Na_2ZnP_2O_7$ [17], respectively.

We continue our previous investigation [15, 16] and search for new Na-based pyrophosphate materials for application in the secondary sodium ion batteries. In the present work the $Na_2Zn_{0.5}Mn_{0.5}P_2O_7$ powder was synthesized by the solid state reaction and ceramics were sintered. The structure studies of the powder were conducted by X-ray diffraction (XRD) in the temperature range from room temperature (RT) to 520 K. The chemical composition of the powder and ceramic samples were investigated by a scanning electron microscope (SEM), an energy dispersive X-ray spectrometer (EDX) and X-ray fluorescence spectroscopy (XFS). The surface of the ceramics was examined by X-ray photoelectron spectroscopy (XPS). The measurements of complex electrical conductivity $\tilde{\sigma} = \sigma' + i\sigma''$, complex impedance $\tilde{\rho} = \rho' - i\rho''$ and complex dielectric permittivity $\tilde{\varepsilon} = \varepsilon' - i\varepsilon''$ of the ceramics were carried out in air in the temperature interval from RT to 700 K and in the frequency range from 10 Hz to 1 GHz.

2. Experiment

The $Na_2Zn_{0.5}Mn_{0.5}P_2O_7$ powder was synthesized by the solid-state reaction method from the stoichiometric amounts of Na_2CO_3, ZnO and MnO (all chemically pure). The precursor was mixed and then a stoichiometric amount of 85% H_3PO_4 (diluted with distilled water 1:1) was added very slowly while mixing. The obtained mixture was heated in silica-carbon crucible at 393 K for 5 h and milled. After milling, the obtained powder was pressed into pellets at 50 MPa. The pellets were heated at 673 K for 4 h and subsequently at 923 K for 6 h. The tubular furnace with steady Ar/H_2 flow was used in all heating steps. After the annealing, the pellet was cooled down to RT in Ar/H_2 atmosphere. The obtained product was milled into ceramic powder.

A *Bruker* D8 X-ray diffractometer equipped with a *MRI Physikalische Geräte GmbH* TC-BASIC heating chamber was used to measure the XRD patterns of the synthesized powder between room temperature and 520 K. During heating and cooling the XRD patterns were recorded with a 20 K temperature step. While changing between two temperature levels the heating and cooling rate was 10 degrees per minute. In order to achieve the thermal equilibrium and completeness of the processes after reaching each temperature, the sample was kept at a selected temperature for 60 or 20 minutes during the heating and cooling processes, respectively. The scan rate for the pattern recording during heating was roughly 0.175 degree per minute, during cooling it was 0.25 degree per minute, at RT and 600 K temperature it was 0.1 degree per minute. The XRD patterns were investigated using $CuK\alpha_1$ radiation in the $2q$ region of 10–60 degrees with a step size of 0.01 degree. Analysis of the measured data was done by the TOPAS v.4.1 software.

The ceramic samples for SEM/EDX and XPS analysis and measurements of electrical properties were sintered. The powder was uniaxially pressed into pellets at 250 MPa. The $Na_2Zn_{0.5}Mn_{0.5}P_2O_7$ pellets were sintered at 953 K for 2 h in air. The density of the ceramics was calculated from geometrical and weight measurements and it was found to be 2.73 g/cm^3. The SEM/EDX (*Hitachi* TM3000) was used for the analysis of the chemical composition of investigated ceramic samples and powder. X-ray fluorescence analysis was performed using a WDXRF spectrometer S4 Pioneer (*Bruker AXS*), equipped with an Rh target X-ray tube (60 kV, 60 mA). The LiF crystal and gas flow (mixture of Ar^+ 10% CH_4) were used. The spectral data were processed with the Spectra Plus software of the S4 device. The element concentrations after the calibration of S4 equipment were calculated automatically.

XPS measurements for the $Na_2Zn_{0.5}Mn_{0.5}P_2O_7$ ceramic sample were performed on an upgraded Vacuum Generator (VG) ESCALAB MkII spectrometer fitted with a new XR4 twin anode. The non-monochromatised AlKα X-ray source was operated at $h\nu$ = 1486.6 eV with 300 W power (20 mA/15 kV) and the pressure in the analysis chamber was lower than $5{\cdot}10^{-7}$ Pa during the spectral acquisition. The spectra were acquired with the electron analyzer pass energy of 20 eV for narrow scans and the resolution of 0.05 eV and with pass energy of 100 eV for survey spectra. All spectra were recorded at the 90° take-off angle and calibrated from the hydrocarbon contamination using the C 1s peak at 284.6 eV. Before the XPS measurements the surface was etched by argon in order to observe the surface state of the sample. Ar^+ ion beam sputtering was performed in the preparation chamber using 2 keV Ar^+ ions bombardment with a beam current density of 20 μA cm^{-2} for a duration of 30, 90 and 390 s. Spectra calibration, processing and fitting routines were done using the AVANTAGE software (5.962) provided by *Thermo VG Scientific*. Core level peaks were analysed using a nonlinear Shirley-type background, and the calculation of the elemental composition was performed on the basis of Scofield's relative sensitivity factors.

Measurements of the electrical properties of $Na_2Zn_{0.5}Mn_{0.5}P_2O_7$ ceramic samples in a low frequency range (10 Hz – 2 MHz) were carried out by the two probe method [18]. The electrodes were fired at 920 K on the sintered cylindrical samples by applying conductive Pt paste (*Gwent Electronics Materials Ltd.*). The measurements in the microwave range ($3{\cdot}10^5$–$3{\cdot}10^9$ Hz) were performed by an *Agilent* Network Analyzer E5062A connected to the coaxial line, and part of the inner conductor of the coaxial line was replaced by the sample. The impedance of the sample was calculated from scattering parameters of such network as in [19]. The temperature was changed in the range 300–700 K during the impedance spectroscopy experiments in the low and high frequency ranges and measured using a digital thermometer TMD90A. The temperature was controlled by a computer connected to a DC power supply.

3. Results and discussion

The analysis of the XRD patterns show that the $Na_2Zn_{0.5}Mn_{0.5}P_2O_7$ powder prepared by the solid state reaction at RT consists of two phases: $Na_2MnP_2O_7$ crystallizes in the triclinic space group $P\bar{1}$ (XRD card 074–2586) as it was summarized in [5], and $Na_2ZnP_2O_7$ crystallizes in the tetragonal space group $P4_2/mmm$ (XRD card 01-070-5836) and it is identical to the one obtained in [12]. The lattice parameters, unit cell volume V, angles α, β, γ, formula units in the unit cell Z and the theoretical density ρ_{th} of both phases at RT are presented in Table 1. The quantitative crystallographic analysis shows that the obtained composite consists of 38.64 wt.% $Na_2MnP_2O_7$ phase and 61.36 wt.% $Na_2ZnP_2O_7$ phase. This composition differs from the one expected from the compound stoichiometry and indicates that a fraction of $Na_2MnP_2O_7$ compound could be present in an amorphous phase and/or that Mn partially replaces Zn in tetragonal $Na_2ZnP_2O_7$ crystallites.

Table 1. Summary of the X-ray diffraction analysis of $Na_2Zn_{0.5}Mn_{0.5}P_2O_7$ powder at room temperature.

Phase	a, Å	b, Å	c, Å	α, deg	β, deg	γ, deg	V, Å^3	Z	ρ_{th}, g/cm^3
$Na_2MnP_2O_7$	9.89(4)	11.08(5)	12.46(3)	148.48	121.98	68.35	595.18(15)	4	3.07
$Na_2ZnP_2O_7$	7.72(5)	10.27(4)	–	–	–	–	612.13(15)	4	3.10

The XRD patterns recorded during the heating and cooling processes do not reveal any appearance or disappearance of the peaks (Fig. 1). As the only certain difference between the patterns at different temperatures is a continuous shift of the peaks towards lower 2θ values during heating and towards higher 2θ values during cooling, it is presumed that there are no changes in the phase composition of the sample and all changes are related to the lattice parameter variation due to the thermal expansion. The temperature dependences of the lattice parameters and the theoretical densities of the $Na_2MnP_2O_7$ and $Na_2ZnP_2O_7$ compounds in the heating and cooling cycles are presented in Fig. 2(a, b), respectively.

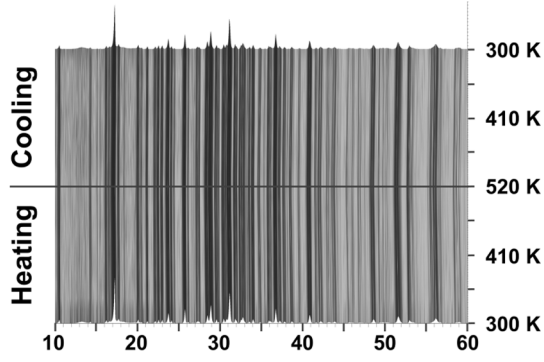

Fig. 1. Pseudo 3D montage of the XRD patterns of $Na_2Zn_{0.5}Mn_{0.5}P_2O_7$ powder during heating and cooling in 300–520 K temperature range.

The lattice parameters of the $Na_2ZnP_2O_7$ phases in the investigated temperature range increase linearly in the heating stage and decrease linearly in the cooling stage. The temperature hysteresis of *a* and *c* lattice parameters during heating and cooling was observed for the $Na_2MnP_2O_7$ phase. The available XRD data does not provide any evidence of the formation of new phases and can be attributed to the evaporation of adsorbed water. Water adsorption at the surface of other similar pyrophosphate ceramics, such as $Na_2MnP_2O_7$ [15] and $NaCsZn_{0.5}Mn_{0.5}P_2O_7$ [16], has also been observed.

The SEM image of the surface of $Na_2Zn_{0.5}Mn_{0.5}P_2O_7$ ceramics is presented in Fig. 3. The grain sizes of the ceramics vary in the range from approximately 3 to 21 μm.

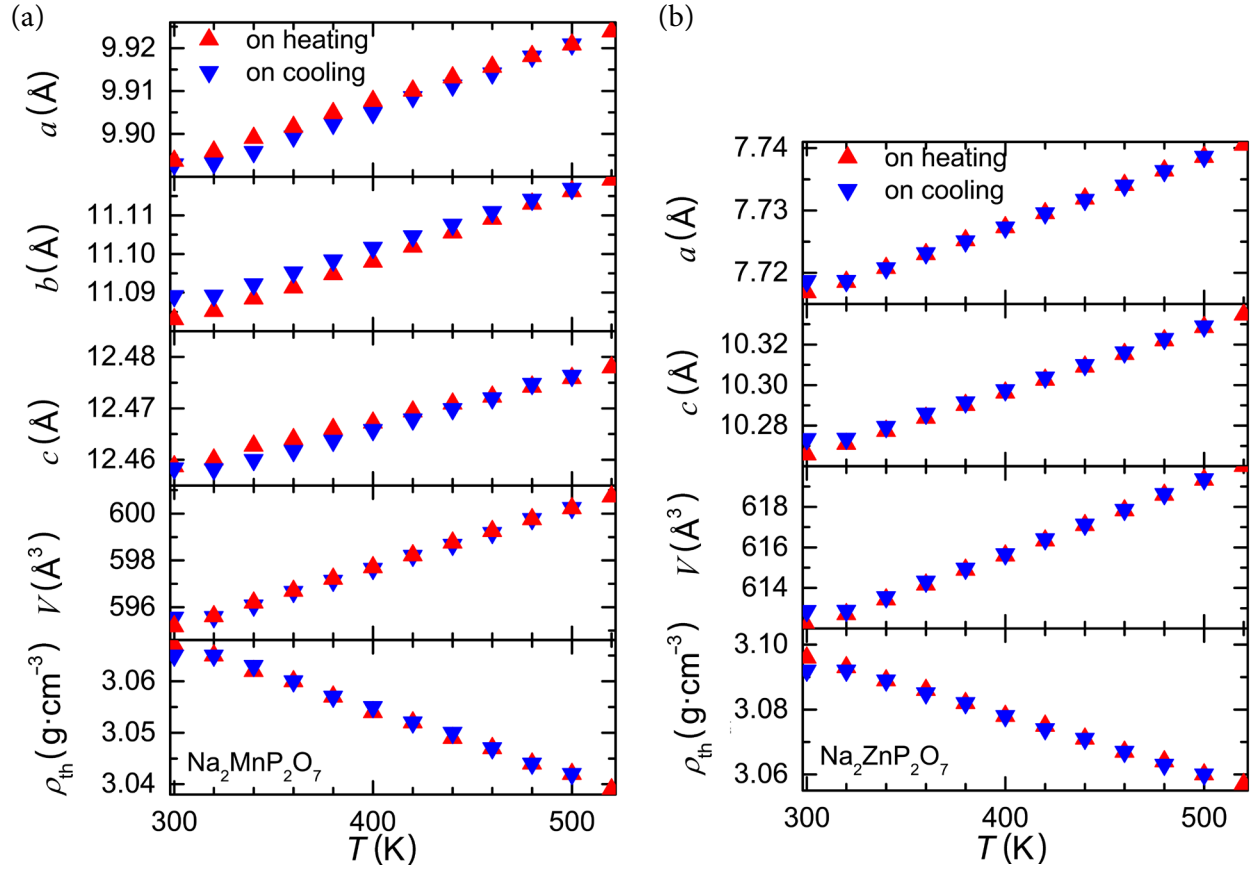

Fig. 2. Temperature dependences of the lattice parameters and theoretical densities of $Na_2MnP_2O_7$ (a) and $Na_2ZnP_2O_7$ (b) compounds during heating and cooling.

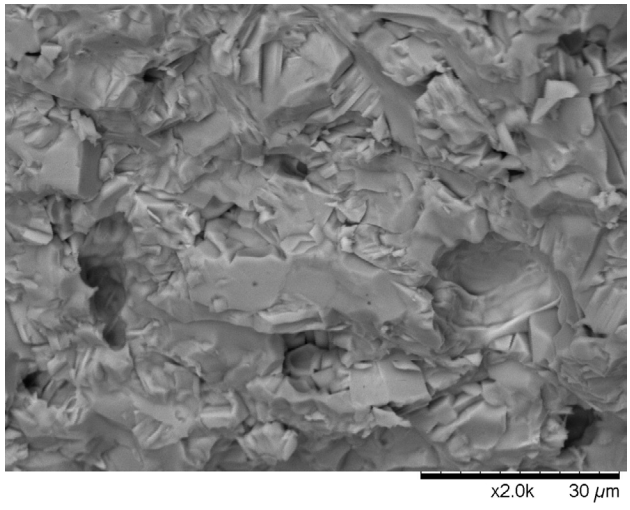

Fig. 3. SEM image of $Na_2Zn_{0.5}Mn_{0.5}P_2O_7$ ceramics.

The experimental density of the composite was measured by direct methods and found to be 2.73 g/cm^3 while the ratio between the density obtained experimentally and calculated theoretically is 88%.

Figure 4 shows the EDX spectra of the $Na_2Zn_{0.5}Mn_{0.5}P_2O_7$ powder and ceramic samples. The calculated theoretical elemental composition and the results of XFS, EDX and XPS spectra analysis of the $Na_2Zn_{0.5}Mn_{0.5}P_2O_7$ powder and ceramic samples are presented in Table 2.

The comparison of the experimental and theoretical elemental composition of $Na_2Zn_{0.5}Mn_{0.5}P_2O_7$ indicates P and Mn deficiency in the ceramic samples and Na excess in the powder. However, the analysis of XPS spectra detected the excess of Zn and Mn after the etching of the ceramic surface. The characteristic Mn 2p and O 1s core level XPS spectra for the 390 s etched surface of $Na_2Zn_{0.5}Mn_{0.5}P_2O_7$ ceramics are shown in Fig. 5 (a, b), respectively.

The Mn $2p_{3/2}$ core level XPS spectra were deconvoluted in three multiple peaks with different binding energy. The peak located at the binding energy 640.05 eV is associated with the Mn^{2+} valence state as in MnO [20]. The multipeak at the binding energy 641.40 eV is related with the Mn^{3+} valence state as in Mn_2O_3 previously reported in [21]. The Mn $2p_{3/2}$ core level peak at 641.90 eV is associated with the Mn^{4+} valence state ion as in MnO_2 [22] and correlated well with the results already published in [23]. In the range 644–648 eV the diffuse MnO shake-up peak is detected. The amounts of the Mn^{2+}, Mn^{3+} and Mn^{4+}

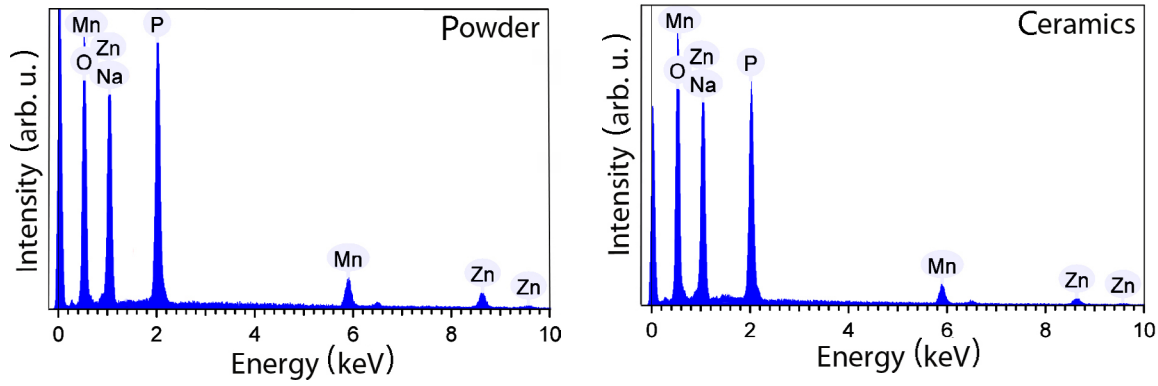

Fig. 4. EDX spectra of $Na_2Zn_{0.5}Mn_{0.5}P_2O_7$ powder and ceramics.

Table 2. Theoretical and experimental elemental composition of $Na_2Zn_{0.5}Mn_{0.5}P_2O_7$ powder and ceramic samples.

Element	Theoretical, wt.%	From XFS, wt.% powder	From EDX, wt.% ceramics	Error, wt.%	From EDX, wt.% powder	Error, wt.%	From XPS, wt.% ** ceramics
Na	16.42	18.90	16.90	0.42	18.04	0.37	16.52
Zn	11.67	11.84	11.16	0.72	11.27	0.63	15.79
Mn	9.81	9.72	8.00	0.29	6.21	0.21	13.27
P	22.12	20.60	20.69	0.32	17.82	0.25	22.79
O	39.98	38.94*	43.25	0.56	46.66	0.50	31.63

* calculated value, ** after Ar^+ ion beam sputtering for 390 s.

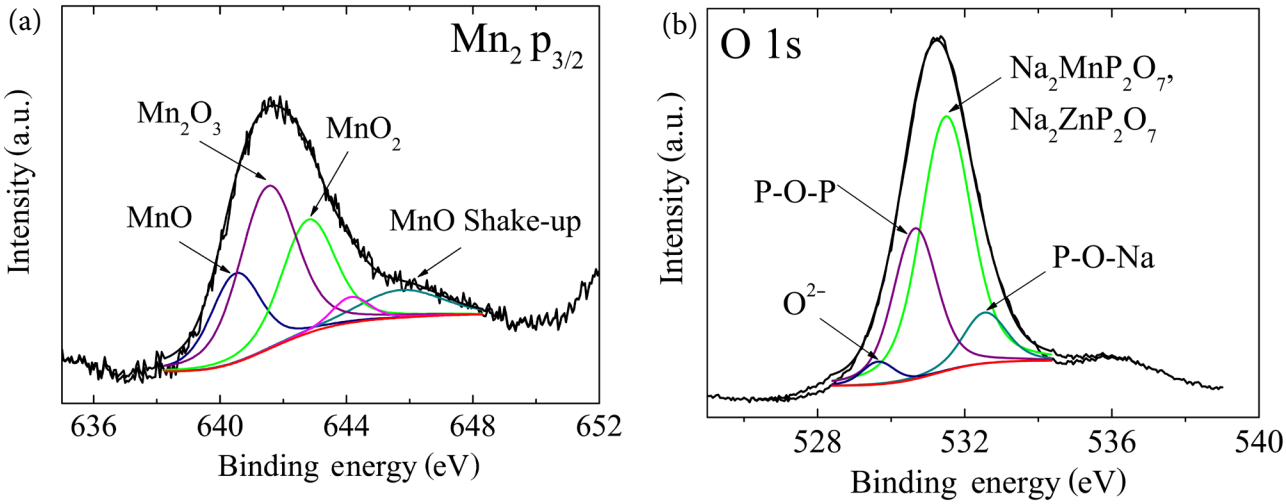

Fig. 5. Mn $2p_{3/2}$ (a) and O 1s (b) core level XPS spectra for the surface of $Na_2Zn_{0.5}Mn_{0.5}P_2O_7$ ceramic.

valence state in the investigated ceramics were 3.6, 5.2 and 4.3 wt.%, respectively. The O 1s spectrum for the $Na_2Zn_{0.5}Mn_{0.5}P_2O_7$ ceramics is of an asymmetric shape, which could be fitted with an intense component and three lower intensity peaks. The highest intensity peak is centered at the binding energy 531.4 eV (amount 16.45 wt.%) and other lower intensity peaks are located at the binding energies 530.65 eV (amount 9.47 wt.%), 532.54 eV (amount 3.53 wt.%) and 529.64 eV (amount 1.03 wt.%). The peak with the highest intensity can be attributed to the lattice oxygen O^{2-} in the $Na_2MnP_2O_7$ and $Na_2ZnP_2O_7$ phases. The peak at the binding energy 530.6 eV represents a structural amount of the OH^- group as in the family of manganite compounds [22]. The peak at the binding energy 532.54 eV can be attributed to the P–O–Na bindings as in [24, 25].

The frequency dependences of the real part of $Na_2Zn_{0.5}Mn_{0.5}P_2O_7$ ceramics complex conductivity (σ'), which were measured at different temperatures, are shown in Fig. 6. A dispersion region was found in the conductivity spectra of $Na_2Zn_{0.5}Mn_{0.5}P_2O_7$ ceramics.

The process is thermally activated and the dispersion region shifts towards higher frequencies as temperature increases in the temperature range 350–700 K. This phenomenon is typical of relaxation type dispersions. The conductivity dispersion above 350 K can be attributed to Na^+ ion migration in the grains of ceramic samples as in [26–28]. The temperature dependences of bulk

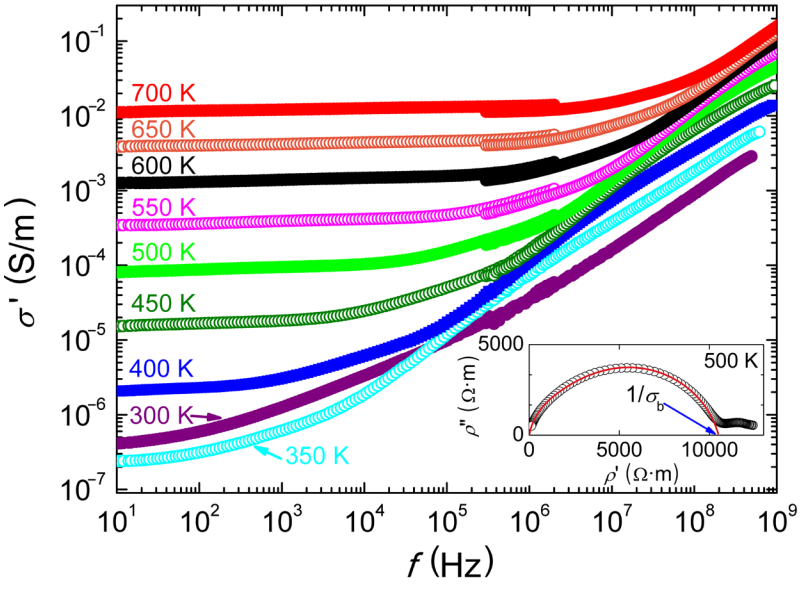

Fig. 6. Frequency dependences of σ' for $Na_2Zn_{0.5}Mn_{0.5}P_2O_7$ ceramics at different temperatures. Inset shows the Nyquist impedance plot at 500 K.

electrical conductivity (σ_b) of the ceramics were derived from Nyquist impedance plots (see inset of Fig. 6). The temperature dependences of σ_b of $Na_2Zn_{0.5}Mn_{0.5}P_2O_7$ ceramics during heating and cooling cycles are presented in Fig. 7.

The non-Arrhenius behaviour of σ_b (1000/T) was observed in the temperature range from 300 to 360 K. The decrease of the $Na_2Zn_{0.5}Mn_{0.5}P_2O_7$ ceramics conductivity in the abovementioned temperature range in the heating stage can be associated with water loss. The conductivity starts to increase rapidly in the cooling stage from 330 K down to 300 K because of adsorbed water. This phenomenon was also observed in $Na_2MnP_2O_7$ [15], $NaCsZn_{0.5}Mn_{0.5}P_2O_7$ [16], $A_{0.9}In_{0.1}P_2O_7$ (A = Sn, Ti) [29] and CeP_2O_7 [30]. A big influence of water on the conductivity at temperatures up to ~350 K is also observed for $Na_2MnP_2O_7$ [15] and $Na_2ZnP_2O_7$ ceramics, their conductivity temperature dependences are presented in Fig. 7 for comparison.

Further conductivity increase with temperature in the temperature interval 350–700 K was described by the Arrhenius law. The data in the graphical representation of conductivity in the logarithmic scale vs reciprocal temperature can be fitted by a straight line, the slope of which is proportional to the activation energy of σ_b. A change of the activation energy ΔE_b of $Na_2Zn_{0.5}Mn_{0.5}P_2O_7$ bulk conductivity is observed in the temperature range from 600 to 630 K. ΔE_b = 0.66 eV in the temperature range from 350 to 600 K, while at temperatures higher than 630 K ΔE_b = 0.83 eV. Knowing that $Na_2Zn_{0.5}Mn_{0.5}P_2O_7$ is the mixed phase material, consisting of $Na_2ZnP_2O_7$ and $Na_2MnP_2O_7$, the latter should be responsible for the change of conductivity activation energy. The phase transition in $Na_2MnP_2O_7$ was observed at 660 K, which led to a step-like conductivity increase in the heating stage. In the $Na_2ZnP_2O_7$ material no phase transitions were found in the whole temperature range of investigation. In the temperature range of 350 to 600 K the conductivity values of $Na_2Zn_{0.5}Mn_{0.5}P_2O_7$ are close to the ones of $Na_2MnP_2O_7$, while at temperature higher than the phase transition, the value of the conductivity of $Na_2Zn_{0.5}Mn_{0.5}P_2O_7$ is mostly determined by lower conductivity of $Na_2ZnP_2O_7$. However, the change of activation energy in the $Na_2Zn_{0.5}Mn_{0.5}P_2O_7$ composite at 630 K is caused by the phase transition taking place in the $Na_2MnP_2O_7$ phase.

The temperature dependences of the real part of dielectric permittivity (ε') and dielectric loss were investigated at a frequency of 1 GHz. This frequency is higher than the Maxwell relaxation frequency ($f_M = \sigma'/2\pi\varepsilon'\varepsilon_0$, where $\varepsilon_0 = 8.85 \times 10^{-12}$ F/m is the dielectric constant of the vacuum) at any measurement temperature, as can be seen from Fig. 8(a). At 630 K the change of the activation energy of f_M was found. The relaxation frequency activation energy in the temperature range 350–630 K is 0.69 eV, and at temperatures from 630 to 700 K it is 0.9 eV. The obtained values are close to the activation energies found from the temperature dependences of bulk conductivity.

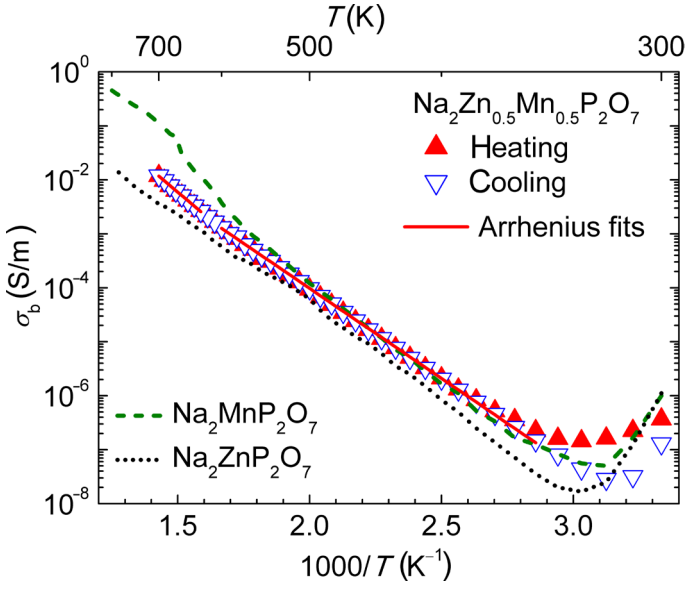

Fig. 7. Temperature dependences of the bulk electrical conductivity of $Na_2Zn_{0.5}Mn_{0.5}P_2O_7$ ceramics during heating and cooling. Conductivities of $Na_2ZnP_2O_7$ and $Na_2MnP_2O_7$ [15] phases are also presented for comparison.

The temperature dependence of the ε' of $Na_2Zn_{0.5}Mn_{0.5}P_2O_7$ ceramics measured at heating and cooling is shown in Fig. 8(b). No difference in the ε' values can be observed comparing heating and cooling data points. This observation suggests that all polarization processes taking place in the bulk of ceramics are reversible. Hence the dielectric permittivity determined at 1 GHz is not connected with the water release which we observe from the conductivity temperature behaviour.

The increase of the value of dielectric permittivity from 8.4 to 12.3 is observed over the whole measured temperature range. The increase of ε' with temperature is caused by contribution of electronic polarization, vibration of the lattice, migration polarization of Na^+ ions in the grains of $Na_2Zn_{0.5}Mn_{0.5}P_2O_7$ ceramics. As the dielectric losses represent conductivity ($\tan\delta = \sigma'/\sigma''$), $\tan\delta$ is shown in the Arrhenius representation. A change of the slope was found at about 630 K, which corresponds to the change of conductivity activation energy, and it was related to the phase transition taking place in the $Na_2MnP_2O_7$ constituent of $Na_2Zn_{0.5}Mn_{0.5}P_2O_7$ ceramics. Besides, we can see that at high frequency (1 GHz) water does not influence ionic transport properties at low temperatures of 300–350 K. So the low temperature conductivity values are caused by surface water diffusion and probably by the contribution of grain boundaries and porosity.

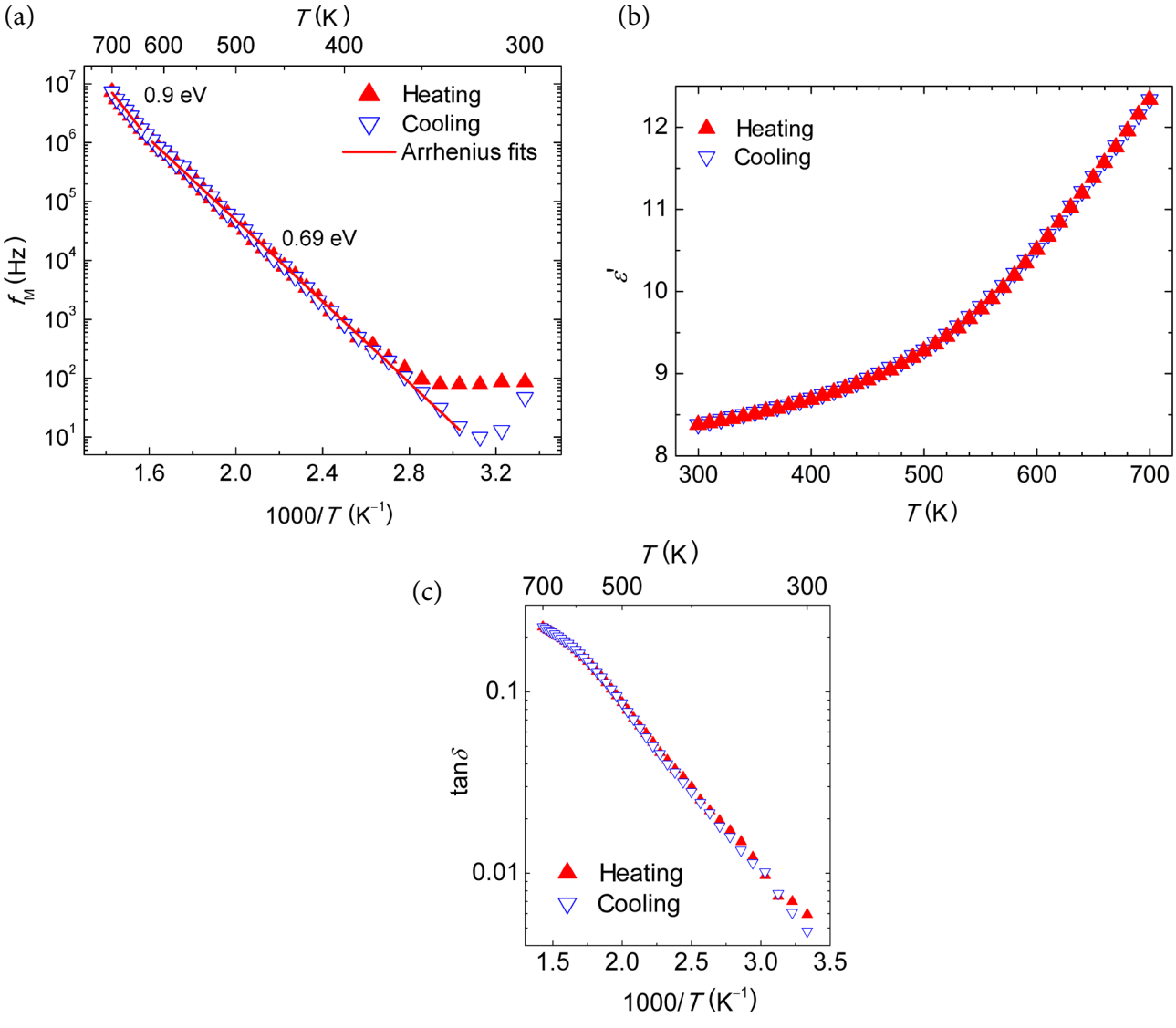

Fig. 8. Temperature dependences of the Maxwell relaxation frequency (a), the real part of complex dielectric permittivity (b) and the dielectric losses (c) of $Na_2Zn_{0.5}Mn_{0.5}P_2O_7$ ceramics measured at 1 GHz in the heating and cooling cycles.

Conclusions

The X-ray diffraction analysis has revealed that the $Na_2Zn_{0.5}Mn_{0.5}P_2O_7$ powder synthesized by the solid state reaction is a mixed phase compound, which consists of $Na_2MnP_2O_7$ (38.64 wt.%) and $Na_2ZnP_2O_7$ (61.36 wt.%) phases. In the temperature interval from 360 to 700 K the total electrical conductivity of $Na_2Zn_{0.5}Mn_{0.5}P_2O_7$ increases with temperature according to the Arrhenius law, but the activation energy change was found at about 630 K. This change was associated with the phase transition taking place in the $Na_2MnP_2O_7$ phase. The temperature hysteresis of the total electrical conductivity value was found in the heating and cooling stages of $Na_2Zn_{0.5}Mn_{0.5}P_2O_7$ ceramics in the temperature range 300–360 K. Non-Arrhenius behaviours of the temperature dependence of conductivity can be associated with dehydration of the samples. The increase of the ε' value with temperature can be caused by contribution of electronic polarization, vibration of the lattices of the mixed phase compound and migration polarization of Na^+ ions in the grains of $Na_2Zn_{0.5}Mn_{0.5}P_2O_7$ ceramics. The investigation of $\tan\delta$ at a frequency of 1 GHz leads to the conclusion that water influences conductivity due to its diffusion on the ceramic surface.

Acknowledgements

The research leading to these results has received funding from the Research Cooperation Project of the Latvian Council of Science No. 666/2014.

References

[1] M. Armand and J.M. Tarascon, Building better batteries, Nature **451**, 652–657 (2008), https://doi.org/doi:10.1038/451652a

[2] J.B. Goodenough and Y. Kim, Challenges for rechargeable Li batteries, Chem. Mater. **22**(3), 587–603 (2010), https://doi.org/10.1021/cm901452z

[3] Z.L. Gong and Y. Yang, Recent advances in the research of polyanion-type cathode materials for Li-ion batteries, Energy Environ. Sci. **4**, 3223–3242 (2011), https://doi.org/10.1039/C0EE00713G

[4] R.A. Shakoor, C.S. Park, A.A. Raja, J. Shin, and R. Kahraman, A mixed iron–manganese based pyrophosphate cathode, $Na_2Fe_{0.5}Mn_{0.5}P_2O_7$, for rechargeable sodium ion batteries, Phys. Chem. Chem. Phys. **18**(5), 3929–3935 (2016), https://doi.org/10.1039/C5CP06836C

[5] Q. Huang and S.J. Hwu, Synthesis and characterization of three new layered phosphates $Na_2MnP_2O_7$, $NaCsMnP_2O_7$ and $NaCsMn_{0.35}Cu_{0.65}P_2O_7$, Inorg. Chem. **37**(22), 5869–5874 (1998), https://doi.org/10.1021/ic980616d

[6] P. Barpanda, T. Ye, M. Avdeev, S.Ch. Chung, and A. Yamada, A new polymorph of $Na_2MnP_2O_7$ as 3.6 V cathode material for sodium-ion batteries, J. Mater. Chem. A **1**(13), 4194–4197 (2013), https://doi.org/10.1039/C3TA10210F

[7] P. Barpanda, G. Liu, Z. Mohamed, Ch.D. Ling, and A. Yamada, Structural, magnetic and electrochemical investigation of novel binary $Na_{2-x}(Fe_{1-y}Mn_y)P_2O_7$ ($0 \le y \le 1$) pyrophosphate compounds for reachable sodium-ion batteries, Solid State Ionics **268**(B), 305–311 (2014), https://doi.org/10.1016/j.ssi.2014.03.011

[8] P. Barpanda, T. Ye, Sh. Nishimura, S.Ch. Chung, Y. Yamada, M. Okubo, H. Zhou, and A. Yamada, Sodium iron pyrophosphate: A novel 3.0 V iron-based cathode for sodium-ion batteries, Electochem. Commun. **24**, 116–119 (2012), https://doi.org/10.1016/j.elecom.2012.08.028

[9] J.M. Clark, P. Barpanda, A. Yamada, and M.S. Islam, Sodium-ion battery cathodes $NaFe_2P_2O_7$ and $Na_2MnP_2O_7$: diffusion behaviour for high rate performance, J. Mater. Chem. A **2**(30), 11807–11812 (2014), https://doi.org/10.1039/C4TA02383H

[10] P. Barpanda, G. Liu, Ch. Ling, M. Tamaru, M. Avdeev, S.Ch. Chung, Y. Yamada, and A. Yamada, $Na_2FeP_2O_7$: A safe cathode for rechargeable sodium-ion batteries, Chem. Mater. **25**(17), 3480–3487 (2013), https://doi.org/10.1021/cm401657c

[11] P. Barpanda, T. Ye, M. Avdeev, Ch.D. Ling, J. Lu, and A. Yamoda, Magnetic structure and properties of the $Na_2CoP_2O_7$ pyrophosphate cathode for sodium-ion batteries: A supersuperexchange-driven non-collinear antiferromagnet, Inorg. Chem. **52**(1), 395–401 (2013), https://doi.org/10.1021/ic302191d

[12] F. Erragh, A. Boukhari, A. Sadel, and E.M. Holt, Disodium zinc pyrophosphate and disodium (europium) zinc pyrophosphate, Acta Cryst. **54**(C), 1373–1376 (1998), https://doi.org/10.1107/S0108270198006246

[13] P. Barpanda, J. Lu, T. Ye, M. Kajiyama, S.Ch. Chung, N. Yabuuchi, S. Komaba, and A. Yamada, A layer-structured $Na_2CoP_2O_7$ pyrophosphate cathode for sodium-ion batteries, RSC Adv. **3**(12), 3857–3860 (2013), https://doi.org/10.1039/C3RA23026K

[14] Ch.S. Park, H. Kim, R.A. Shakoor, E. Yang, S.Y. Lim, R. Kahraman, Y. Jung, and J.W. Choi, Anomalous manganese activation of a pyrophosphate cathode in sodium ion batteries: A combined experimental and theoretical study, J. Am. Chem. Soc. **135**(7), 2787–2792 (2013), https://doi.org/10.1021/ja312044k

[15] S. Daugėla, T. Šalkus, A. Kežionis, V. Venckutė, D. Valdnice, A. Dindune, M. Barre, and A.F. Orliukas, Anomalous temperature-dependent electrical properties of $Na_2MnP_2O_7$, Solid State Ionics **302**, 72–76 (2017), https://doi.org/10.1016/j.ssi.2016.12.020

[16] A.F. Orliukas, V. Venckutė, S. Daugėla, A. Kežionis, A. Dindune, D. Valdniece, J. Ronis, M. Lelis, M. Mosiałek, and T. Šalkus, Synthesis, structure and impedance spectroscopy of $NaCsZn_{0.5}Mn_{0.5}P_2O_7$ pyrophosphate ceramics, Solid State Ionics **302**, 92–97 (2017), https://doi.org/10.1016/j.ssi.2016.12.009

[17] S. Chouaib, A.B. Bhaiem, and K. Guidara, Dielectric relaxation and ionic conductivity studies of $Na_2ZnP_2O_7$, Bull. Mater. Sci. **34**(4), 915–920 (2011), https://doi.org/10.1007/s12034-011-0214-1

[18] T. Šalkus, A. Kežionis, V. Kazlauskienė, J. Miškinis, A. Dindune, Z. Kanepe, J. Ronis, and A.F. Orliukas, Surface and impedance spectroscopy studies of $Li_{2.8}Sc_{1.8-y}Y_yZr_{0.2}(PO_4)_3$, Matter. Sci. Eng. B **172**(2), 156–162 (2010), https://doi.org/10.1016/j.mseb.2010.05.002

[19] A. Kežionis, E. Kazakevičius, T. Šalkus, and A.F. Orliukas, Broadband high frequency impedance spectrometer with working temperatures up to 1200 K, Solid State Ionics **188**(1), 110–113 (2011), https://doi.org/10.1016/j.ssi.2010.09.034

[20] V. Di Castro and G. Polzonetti, XPS study of MnO oxidation, J. Electron. Spectrosc. Relat. Phenom. **48**(1), 117–123 (1989), https://doi.org/10.1016/0368-2048(89)80009-X

[21] R.P. Gupta and S.K. Sen, Calculation of multiplet structure of core *p*-vacancy levels, Phys. Rev. B **10**(1), 71–77 (1974), https://doi.org/10.1103/PhysRevB.10.71

[22] H.W. Nesbitt and D. Banerjee, Interpretation of XPS Mn(2p) spectra of Mn oxyhydroxides and constraints on the mechanism of MnO_2 precipitation, Am. Mineral. **83**(3–4), 305–315 (1998), https://doi.org/10.2138/am-1998-3-414

[23] C.N.R. Rao, D.D. Sarma, S. Vasudevan, and M.S. Gegde, Study of transition metal oxides by photoelectron spectroscopy, Proc. R. Soc. A **367**(1729), 239–262 (1979), https://doi.org/10.1098/rspa.1979.0085

[24] N.S. McIntyre and D.G. Zetaruk, X-ray photoelectron spectroscopy studies of iron oxides, Anal. Chem. **49**(11), 1521–1529 (1977), https://doi.org/10.1021/ac50019a016

[25] A.R. Pratt, I.J. Muir, and H.W. Nesbitt, X-ray photoelectron and Auger electron spectroscopic studies of pyrrhotite and mechanism of air oxidation, Geochim. Cosmochim. Acta **58**(2), 827–841 (1994), https://doi.org/10.1016/0016-7037(94)90508-8

[26] E. Kazakevičius, A. Kežionis, L. Žukauskaitė, M. Barre, T. Šalkus, A. Žalga, A. Selskis, and A. Orliukas, Characterization of $Na_{1.3}Al_{0.3}Zr_{1.7}(PO_4)_3$ solid electrolyte ceramics by impedance spectroscopy, Solid State Ionics **271**, 128–133 (2015), https://doi.org/10.1016/j.ssi.2014.09.038

[27] E. Kazakevičius, A. Kežionis, L. Žukauskaitė, M. Barre, T. Šalkus, and A.F. Orliukas, Characterization of NASICON-type Na solid electrolyte ceramics by impedance spectroscopy, Funct. Mater. Lett. **7**(6), 1440002 (2014), https://doi.org/10.1142/S1793604714400025

[28] W. Bogusz, J.R. Dygas, F. Krok, A. Kezionis, R. Sobiestianskas, E. Kazakevicius, and A.F. Orliukas, Electrical conductivity dispersion in

Co-doped NASICON samples, Phys. Stat. Sol. A **183**(2), 323–330 (2001), https://doi.org/10.1002/1521-396X(200102)183:2<323::AID-PSSA323>3.0.CO;2-6

[29] T. Shirai, S. Sotou, Y. Saito, M. Saito, J. Kuwano, and H. Shiroihi, Proton conducting solid electrolytes based on diphosphates, Phosporus Research Bull. **21**, 31 (2007), https://doi.org/10.3363/prb.21.31

[30] X. Sun, S. Wang, Z. Wang, X. Ye, T. Wen, and F. Huang, Proton conductivity of CeP_2O_7 for intermediate temperature fuel cells, Solid State Ionics **179**(21–26), 1138–1141 (2008), https://doi.org/10.1016/j.ssi.2008.01.046

$Na_2Zn_{0,5}Mn_{0,5}P_2O_7$ KERAMIKOS GAMYBA BEI STRUKTŪROS, PAVIRŠIAUS IR ĮMPEDANSO SPEKTROSKOPIJOS TYRIMAI

V. Venckutė [a], A. Dindune [b], D. Valdniece [b], A. Krūmiņa [b], M. Lelis [c], V. Jasulaitienė [d], A. Maneikis [d], S. Daugėla [a], T. Šalkus [a], A. Kežionis [a], A.F. Orliukas [a]

[a] *Vilniaus universiteto Fizikos fakultetas, Vilnius, Lietuva*

[b] *Rygos technikos universiteto Neorganinės chemijos institutas, Ryga, Latvija*

[c] *Lietuvos energetikos instituto Vandenilio energetikos technologijų centras, Kaunas, Lietuva*

[d] *Fizinių ir technologijos mokslų centras, Vilnius, Lietuva*

Santrauka

Darbe $Na_2Zn_{0,5}Mn_{0,5}P_2O_7$ milteliai buvo sintezuoti kietųjų fazių reakcijos metodu. XRD analizė parodė, kad $Na_2Zn_{0,5}Mn_{0,5}P_2O_7$ susideda iš dviejų fazių: triklininės $Na_2MnP_2O_7$ (erdvinė grupė $P\bar{1}$) ir tetragoninės $Na_2ZnP_2O_7$ (erdvinė grupė $P4_2/mmm$). Skaičiuojant pagal masę gautos koncentracijos atitinkamai 38,64 ir 61,36 %. Cheminė miltelių ir iškeptos keramikos sudėtis tyrinėta EDX bei XFS spektroskopijos būdais. Paviršius tyrinėtas XPS spektrometru. Kaip parodė SEM nuotrauka, $Na_2Zn_{0,5}Mn_{0,5}P_2O_7$ keramikos kristalitų dydžiai varijuoja nuo 3 iki 21 μm.

Bandinėliai matuoti impedansą gauti keramikos miltelius suspaudžiant į tabletes 200 MPa slėgiu. $Na_2Zn_{0,5}Mn_{0,5}P_2O_7$ keramikos kepinimo temperatūra 953 K, trukmė – 2 h. Gauto keramiko stankis – 2,73 g/cm^3. Impedanso spektroskopijai matuoti ant cilindro formos bandinėlių uždėta platinos pasta ir atkaitinta 920 K temperatūroje.

Atliekant impedanso matavimus, realiosios laidumo dalies priklausomybė nuo dažnio $Na_2Zn_{0,5}Mn_{0,5}P_2O_7$ keramikoje rodo dispersijos sritį, kuri pasislenka į aukštesnių dažnių pusę kylant temperatūrai nuo 350 iki 700 K. Tai yra tipiška relaksacinio tipo dispersija. Laidumo dispersija per 350 K siejama su Na^+ jonų pernaša keramikos granulėse. Intervale nuo 300 iki 360 K fiksuotas nukrypimas nuo Arenijaus dėsnio. Kaitinimo stadijos metu kylant temperatūrai nuo 300 iki 350 K mažėjo laidumas. Tai susiję su vandens pasišalinimu iš keramikos. Panaši anomalija pasireiškė ir vėsinimo metu: intervale nuo 330 iki 300 K staigiai pradėjo didėti keramikos laidumas dėl vandens adsorbcijos. Panašios anomalijos 300–360 K intervale stebėtos ir tiriant $Na_2MnP_2O_7$, $NaCsZnP_2O_7$ bei $Na_2ZnP_2O_7$ keramikas.

Temperatūrų intervale nuo 600 iki 630 K pastebėtas $Na_2Zn_{0,5}Mn_{0,5}P_2O_7$ kristalitų laidumo aktyvacijos energijos pasikeitimas nuo 0,7 eV, kai temperatūra 350–600 K, iki 0,9 eV, kai temperatūra didesnė nei 630 K. Šis pasikeitimas siejamas su faziniu virsmu $Na_2MnP_2O_7$ fazėje.

Visame tirtajame temperatūrų intervale nuo 300 iki 700 K pastebėtas dielektrinės skvarbos didėjimas kaitinant keramiką. ε' didėjimas kylant temperatūrai priklauso nuo elektroninės poliarizacijos, gardelės virpesių ir Na^+ jonų migracinės poliarizacijos $Na_2Zn_{0,5}Mn_{0,5}P_2O_7$ kristalituose.